Crystal Structure of *Escherichia coli* Fdx, an Adrenodoxin-Type Ferredoxin Involved in the Assembly of Iron−Sulfur Clusters†

Yoshimitsu Kakuta, Tatsuya Horio, Yasuhiro Takahashi, and Keiichi Fukuyama*

Department of Biology, Graduate School of Science, Osaka University, 1-1 Machikaneyama, Toyonaka, Osaka 560-0043, Japan

Received March 16, 2001; Revised Manuscript Received May 30, 2001

ABSTRACT: *Escherichia coli* ferredoxin (Fdx) is an adrenodoxin-type [2Fe-2S] ferredoxin. Recent genetic analyses show that it has an esssential role in the maturation of various iron−sulfur (Fe−S) proteins. Fdx probably functions as a component of the complex machinery responsible for the biogenesis of Fe−S clusters. Its crystal structure was determined by the multiple-wavelength anomalous dispersion method using the iron atoms in the [2Fe-2S] cluster of the protein and then refined to R and R_{free} values of 0.255 and 0.278, respectively, at 1.7 Å resolution. The structure of Fdx is similar to the structures of bovine adrenodoxin (Adx) and *Pseudomonas putida* putidaredoxin (Pdx) whose respective root-mean-square deviations of the corresponding Cα atoms are 1.8 and 2.2 Å. This analysis also revealed the structure of the C-terminal residues protruding into the solvent, which is missing in Adx and Pdx. The [2Fe-2S] cluster is located at the edge of the molecule and bonds with the Sγ atoms of Cys42, Cys48, Cys51, and Cys87. Electrostatic potential analysis showed that the surface of Fdx has two negatively charged areas separated by a hydrophobic lane. One is conserved on the surface of Adx which is an area of interaction with adrenodoxin reductase. Cys46 is located on the molecular surface in the vicinity of the [2Fe-2S] cluster, an indication that it may be involved in Fe−S cluster formation.

Ferredoxins (Fds)[1] are small, acidic, electron transfer proteins that are ubiquitous in biological redox systems. They have either [4Fe-4S], [3Fe-4S], or [2Fe-2S] cluster, whose reduction potential is highly negative (−300 mV or less) (*1*−*3*). Among them, Fds with one [2Fe-2S] cluster per molecule are present in plants, animals, and bacteria, and form a distinct 2Fe−Fd family (*2*, *4*). They have four conserved cysteine residues to which the [2Fe-2S] cluster is ligated, but their amino acid sequences differ considerably depending on the biological processes in which they are involved. One distinct subfamily is comprised of adrenodoxin (Adx) found in animals and putidaredoxin (Pdx) in *Pseudomonas putida*, both of which are involved in the hydroxylase system. Adx, located in the adrenal cortex mitochondria, is involved in the synthesis of steroid hormones in which it transfers electrons from NADPH-dependent reductase to cytochromes P450, whereas Pdx is involved in electron transfer to a cytochrome P450 that hydroxylates camphor to produce a carbon source for bacterial growth (*5*−*7*). The other major 2Fe−Fd subfamily consists of the plant-type Fds present in plants and algae, which function in photosynthesis by transferring electrons from photosystem I to Fd-dependent enzymes, such as Fd-$NADP^+$ reductase and sulfite reductase (*8*). Although the degree of similarity in the amino acid sequences between the two Fd subfamilies is low, the polypeptide chains of the 2Fe−Fd family have a common folding motif, designated as the β-grasp (*9*) or UB-fold (*10*). Adx and Pdx have insertions of amino acid residues at several sites relative to the plant-type Fds (*11*, *12*), their molecular weights being nearly 13K, ∼2K larger than those of the plant-type Fds.

Two members of the Adx/Pdx subfamily, Fdx in *Escherichia coli* and Yah1 in yeast mitochondria, have attracted much attention in recent years. Genetic studies have shown they have a crucial role in the biogenesis of Fe−S clusters. The gene encoding bacterial Fdx is located in the *isc* (iron−sulfur cluster) operon, in which eight genes are clustered (*13*). Overexpression of the entire operon improves the cellular ability for Fe−S cluster biosynthesis, leading to a marked increase in the yield of recombinant Fe−S proteins (*14*). The *fdx* gene, together with *iscS*, *iscU*, *iscA*, *hscB*, and *hscA* in the operon, is crucial for the efficient biosynthesis of Fe−S clusters in *E. coli* (*15*, *16*). The biosynthesis of the Fe−S cluster therefore is a complex process that involves numerous components, including Fdx. Similar machinery has been identified in yeast mitochondria, in which homologues of bacterial IscS, IscU, IscA, HscB, HscA, and Fdx (Nfs1p, Isu1p and Isu2p, Isa1p and Isa2p, Jac1p, Ssq1p, and Yah1p, respectively) participate in the maturation of mitochndrial and cytosolic Fe−S proteins (for recent reviews, see refs *17* and *18*). The *YAH1* gene is indispensable for viability of yeast cells as in the case for other yeast genes involved in Fe−S cluster formation (*17*−*19*). Depletion of Yah1p causes a marked decrease in the activities of Fe−S proteins (*20*).

† This work was supported in part by Grants-in-Aid for Scientific Reseatch on Priority Areas (Molecular Biometallics Grant 10129219 and Biological Machinery Grant 11169223) from the Ministry of Education, Culture, Sports, Science and Technology of Japan to K.F., by the Sakabe Project of TARA (Tsukuba Advanced Research Alliance) of the University of Tsukuba, and by a grant from the Japan Foundation for Applied Enzymology.

* To whom correspondence should be addressed. Telephone: +81-6-6850-5422. Fax: +81-6-6850-5425. E-mail: fukuyama@bio.sci.osaka-u.ac.jp.

[1] Abbreviations: Fe−S, iron−sulfur; Fd, ferredoxin; Adx, adrenodoxin; Pdx, putidaredoxin; AR, adrenodoxin reductase; PR, putidaredoxin reductase; rms, root-mean-square.

10.1021/bi010544t CCC: $20.00
Published on Web 08/21/2001

Fdx and its closely related protein have been purified from *E. coli* and *Azotobacter vinelandii*, and their biochemical and spectroscopic characteristics have been shown to be similar to those of Adx and Pdx (*21*, *22*). *E. coli* Fdx has 111 amino acid residues (*23*), and its sequence is ~40% identical to that of yeast Yah1p and ≤30% identical to those of Adx and Pdx (*15*). Despite the fact that Fdx has a redox active [2Fe-2S] cluster with a reduction potential of −380 mV, it is incapable of replacing Pdx in the electron transfer to camphor-hydroxylating cytochrome P450 (*21*). Similarly, human Adx cannot functionally complement the deletion of the yeast *YAH1* gene (*19*). Apparently, these proteins evolved from a common ancestral protein but diverged for specific functions. Until now, very little has been known about the biochemical reaction in which Fdx/Yah1p is directly involved. One possibility is that the proteins donate electrons to one of the steps of the Fe−S cluster biosynthesis that requires the reducing equivalents. Accordingly, several amino acids in the vicinity of the [2Fe-2S] cluster should interact with other proteins, or with iron and sulfur atoms, producing a function for this class of proteins distinct from that of Adx or Pdx.

To shed light on the functional role of Fdx, we determined the crystal structure of Fdx at 1.7 Å resolution. We describe the structural characteristics of Fdx on the basis of a comparison of the primary and tertiary structures of related proteins, and discuss its possible function.

EXPERIMENTAL PROCEDURES

Protein Expression and Purification. Fdx was overexpressed under coexpression with the *isc* operon, as described previously (*14*). *E. coli* C41(DE3) cells transformed with pET21-Fdx and pRK1SC plasmids were grown in Terrific broth supplemented with 0.1 mg/mL ferric ammonium citrate. Expression was induced with 0.5 mM IPTG and allowed to continue for 19 h at 28 °C. Fdx was purified by ammonium sulfate fractionation, hydrophobic chromatography (Butyl-Toyopearl 650M), and anion-exchange chromatography (DEAE-Toyopearl 650M). The overall yield of purified Fdx was ~200 mg/L of cluture. The brownish Fdx has an absorption spectrum characteristic of [2Fe-2S] Fds with peaks at 280, 339 (broad), 415, and 459 nm ($A_{415}/A_{280} = 0.6$).

Crystallization. Crystallization conditions of Fdx were surveyed extensively by the hanging-drop vapor diffusion and dialysis methods at a protein concentration of 20 mg/mL. Four forms of well-shaped crystals were obtained, but except for one, all gave diffuse diffraction spots and/or had extremely high mosaicity. Rhombohedral crystals suitable for X-ray analysis were obtained when 100 mM Tris-HCl buffer (pH 7.5) containing 33% polyethylene glycol 4000, 5% 2-butanol, and 80 mM $MgCl_2$ was used as the reservoir solution. When the protein solution was mixed with an equal volume of reservoir solution and equilibrated against it at 23 °C, crystals were grown to a size of 0.2 mm × 0.2 mm × 0.15 mm in 2 days. These crystals were sensitive to a change in temperature.

Crystallographic Data Collection and Processing. The crystals could be flash-cooled successfully without being transferred to a cryoprotectant solution. All diffraction data were collected by the oscillation method at 100 K on a MAR CCD detector at beamline BL41XU of SPring-8, Japan. The crystals were trigonal, in space group *R*3, with the following unit cell dimensions: $a = b = 107.3$ Å and $c = 85.2$ Å. The asymmetric unit was expected to have three Fdx molecules ($V_M = 2.6$ Å^3/Da), which was confirmed by the subsequent analysis. For the MAD phasing, two data sets were collected at wavelengths of 1.74 and 1.00 Å from one crystal, and for structural refinement, one data set at 0.70 Å was collected from another crystal (Table 1). Both crystals were mounted on the goniometer in a random orientation. Diffraction images were processed with MOSFLM (*25*), and the intensities were scaled with SCALA (*26*). Each data set was processed and scaled independently.

Table 1: Data Collection and Refinement Statistics

	Data Collection		
	peak	remote	high-resolution
wavelength (Å)	1.74	1.00	0.70
resolution (Å)	20.0−2.8	20.0−2.0	20.0−1.7
oscillation angle/frame (deg)	2.0	2.0	0.9
no. of measured reflections	47654	158612	155486
no. of unique reflections[a]	16947	49291	40083
completeness (%)[b]	99.1 (94.2)	99.9 (99.5)	98.7 (99.6)
redundancy[b]	2.8 (1.2)	3.2 (3.1)	3.9 (2.3)
R_{merge} (%)[b,c]	7.3 (12.3)	5.5 (21.5)	6.6 (27.3)
phasing power[b,d]	1.91 (0.71)	1.18 (0.52)	

Refinement Statistics	
resolution (Å)	20.0−1.7
R/R_{free} (%)[e]	25.5/27.8
no. of refined atoms[f]	2665 (155)
rms deviations from ideality	
bond lengths (Å)	0.005
bond angles (deg)	1.4
dihedral angles (deg)	23.4
improper angles (deg)	0.74
Ramachandran plot (%)	
most favored regions	86.2
additional allowed regions	13.1
generously allowed regions	0.7

[a] For the peak and remote data sets, Bijvoet pairs are treated separately, whereas for the high-resolution data set, their intensities are averaged. [b] Values in parentheses are for the highest-resolution shell. [c] $R_{merge} = \sum_{hkl}\sum_i|I_i(hkl) - \langle I(hkl)\rangle|/\sum_{hkl}\sum_i I_i(hkl)$. [d] Phasing power is the mean anomalous signal divided by the lack-of-closure error. [e] R_{free} was calculated for 10% of the reflections randomly excluded from the refinement. [f] The number in parenthses is the number of water molecules.

Structure Determination and Refinement. Both the Bijvoet and dispersive difference Patterson maps had identical peaks that correspond to vectors between three [2Fe-2S] clusters per asymmetric unit. Refinement of these sites, MAD phasing, and improvement of the electron density by solvent flipping were carried out with CNS (*27*). The polyalanine model of Adx (PDB entry 1AYF) was fitted to one of the two enantiomer-related maps using the program O (*28*), in which substantial change in the main chain conformation was required. Individual iron atoms in each cluster were located on the electron density map at 3.0 Å resolution calculated from the phase angles that were derived from the polypeptide model. These iron sites were consistent with those expected from the orientation of the cluster in the Adx molecule. MAD phasing based on the individual iron sites improved the overall figure of merit from 0.46 to 0.62, in particular for reflections at high resolution (from 0.15 to 0.37 for 3.13−3.0 Å data). The map obtained after solvent flipping enabled us to build a model according to the known amino

acid sequence. This model was refined by alternate application of model revision/water location against $2F_o - F_c$ and $F_o - F_c$ maps and simulated annealing using the high-resolution data. Resolution was extended stepwise to 1.7 Å. The refinement statistics are given in Table 1. The coordinates have been deposited in the Protein Data Bank as entry 1I7H.

RESULTS AND DISCUSSION

Structure Determination. The crystal structure of Fdx was determined by the MAD method using the anomalous scattering of the iron atoms in the [2Fe-2S] cluster, and then refined at 1.7 Å resolution to an R of 25.5% and an R_{free} of 27.8%. There are three molecules (A, B, and C) per asymmeric unit, the solvent content of the unit cell being estimated as ~51%. Of 111 residues in Fdx, residues 2−110 could be built in the A molecule, and residues 2−109 in the B and C molecules. The final model has a total of 2513 protein atoms and 155 water molecules. The Ramachandran plot indicates that, except for Thr92, all residues are in either the most favored or additional allowed regions. Only Thr92 is in the generously allowed region, its ϕ and ψ angles in molecules A, B, and C being $-117 \pm 7°$ and $-102 \pm 7°$, respectively. The environments of Thr92 are conserved in the three molecules, and both the side and main chains of Thr92 are involved in hydrogen bonds with neighboring segments of the polypeptide chains: NH(Thr92)···Wat···Oγ(Ser61), O(Thr92)···OγH(Ser23), and Oγ(Thr92)···O(Ser61). In addition, the water molecule hydrogen bonded to NH(Thr92) is connected to O(Glu94). Therefore, the present conformation of Thr92 probably contributes to maintaining the correct folding of the Fdx molecule.

Overall Structure. The overall structure of Fdx is shown by the ribbon drawing in Figure 1. The [2Fe-2S] cluster is located at the edge of the molecule. The three molecules (A, B, and C) in the asymmetric unit are very similar. The Cα atoms of residues 2−109 between the A and B molecules, the A and C molecules, and the B and C molecules are superimposed with respective root-mean-square (rms) deviations of 0.48, 0.28, and 0.47 Å.

Fdx is an (α+β)-protein consisting of a core (residues 2−58 and 86−100) and protruding (residues 59−85) domains, and a protruding tail (residues 101−110). The folding of the core domain is classified in the β-grasp (*9*) or UB-fold (*10*) which is characterized as having a β-sheet comprised of four β-strands and one α-helix flanking the sheet (βA, βB, βD, βH, and αC in Figure 1). Both the core and protruding domains are present in electron transfer proteins, including the plant-type Fds (*30*−*35*), halophilic 2Fe−Fd (*36*), and the C-terminal domain of phthalate dioxygenase reductase (*37*). Only the β-grasp/UB-fold motif of the core domain, however, is found in such functionally unrelated proteins as ubiquitin (*38*), the immunoglobulin-binding domain of protein G (*39*), and the Ras-binding domain of human c-Raf1 (*40*).

Secondary structures in the protruding domain of Fdx (αE, αF, and short βG) are conserved in bovine Adx (*13*) and *Pseudomonas* Pdx (*12*, *41*) but not in the plant-type Fds. Although a one-turn helix is present in a position similar to that of αF in the subfamily of the plant-type Fds, its orientation differs from that of αF (*30*−*35*). Short αE is absent in the plant-type Fds. Accordingly, the folding of Fdx is most similar to the foldings of Adx and Pdx. The locations and orientations of αE, αF, and βG are characteristic in the Fdx/Adx/Pdx subfamily.

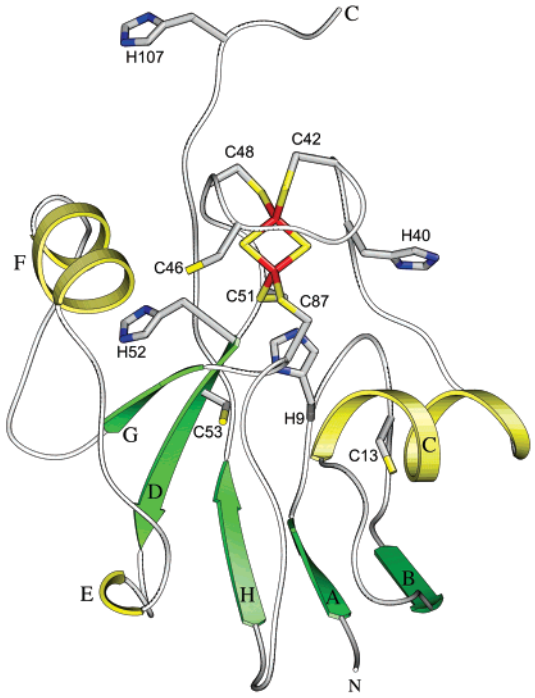

FIGURE 1: Ribbon representation of the Fdx protein. Helices are shown in yellow, strands in green, and random coils in gray. The [2Fe-2S] cluster is shown as a stick representation (Fe, red; S, yellow). Side chains of cysteine and histidine residues are also shown. The figure was drawn using SETOR (*49*).

FIGURE 2: Sequence alignment of Fdx, Adx, and Pdx. This alignment is based on the three-dimensional structures of Fdx, Adx, and Pdx. The secondary structures are shown with green arrows (β-strand) and yellow boxes (α-helix) above the sequence. The secondary structure of Fdx was analyzed using the program PROCHECK (*29*). Residues given in red are conserved in at least two proteins, and residues given in blue are ligands to the [2Fe-2S] cluster. Residues shown in gray are truncated or disordered in the crystal structures. Putative residues that interact with reductase are boxed in red.

Comparison to Bovine Adrenodoxin and P. putida Putidaredoxin. The primary structures of bovine Adx and *P. putida* Pdx are shown in Figure 2. Fdx is ~30% homologous to both Adx and Pdx. Adx consists of 128 residues, and the structure of its truncated form (residues 4−108) was determined by X-ray crystallography (*13*). Pdx, however, consists of 106 residues, and its structure was determined by NMR spectroscopy (*12*, *41*). A superposition of the Cα traces of Fdx and Adx is shown in Figure 3. The overall

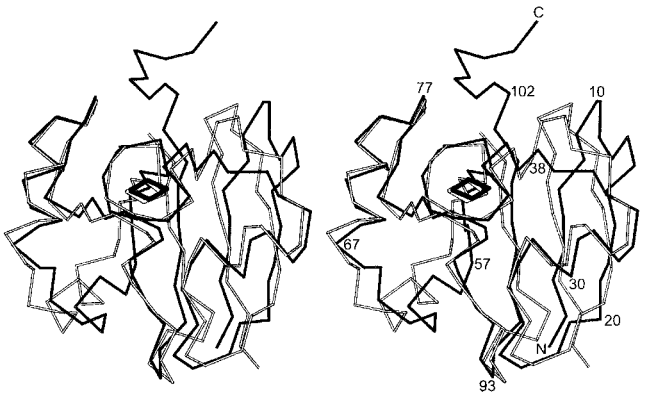

FIGURE 3: Superposition of Fdx on Adx. Cα traces of these two proteins with an [2Fe-2S] cluster: black bond, Fdx; white bond, Adx.

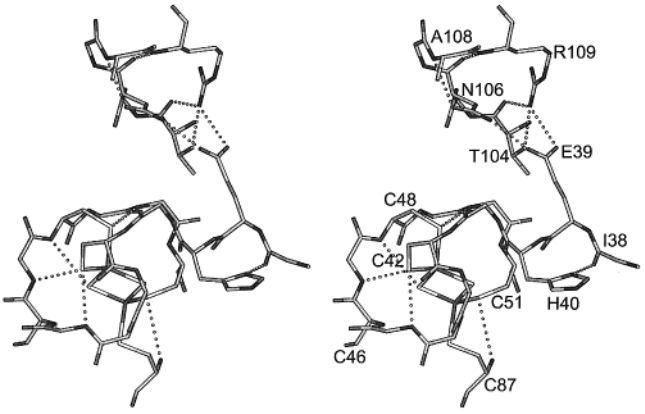

FIGURE 4: Closeup view of the vicinity of the [2Fe-2S] cluster and C-terminal tail. Hydrogen bonds that maintain the C-terminal tail that projects into the solvent and NH···S hydrogen bonds are shown as dotted lines: N(Ser45)···Sγ(Cys42) (3.3 Å), N(Ala47)···Sγ(Cys42) (3.3 Å), N(Cys48)···S1 (3.5 Å), N(Thr50)···Sγ(Cys48) (3.5 Å), and N(Cys87)···Sγ(Cys51) (3.6 Å). The figure was drawn with SETOR (*49*).

foldings of Fdx, Adx, and Pdx are similar; the main difference among the secondary structures is that 3_{10}-helices H and I found in Adx are lacking in Fdx. When the entire molecules are superimposed, the rms deviations between the corresponding Cα atoms are 1.8 Å for the Fdx−Adx pair and 2.2 Å for the Fdx−Pdx pair. Except for the N- and C-termini, insertions/deletions of the amino acid residues in Fdx relative to Adx occur at four sites: insertion of three residues between βA and βB, deletion of two residues between αC and the cluster binding loop, deletion of one residue between βD and αE, and deletion of two residues before βH (Figures 2 and 3). These insertions/deletions produce significant conformational change in the segment where they occur. Moreover, the third one causes additional conformational change in the N-terminal half of the protruding domain. Most of the conformational changes produced by these insertins/deletions, however, are restricted in local segments, the arrangement of the secondary structures in the core domain being affected little.

Fdx and Adx have C-terminal extensions rich in hydrophilic amino acid residues (Figures 2 and 4). It is noteworthy that, unlike in Adx, most of the C-terminal residues are visible in Fdx, and are located near the [2Fe-2S] cluster. The 20 C-terminal residues of Adx beyond Pro108 (Pro101 in Fdx numbering) have been truncated (*13*). Although the crystal structure of full-length Adx was determined recently, only a few of the additional residues after the C-terminus of truncated Adx became visible (*42*). Residues Ile105−Glu110 in the protruding tail have internal hydrogen bonds as well as hydrogen bonds to Glu39 in the core domain [Oε1(Glu39)···N2(Arg109) and Oε2-(Glu39)···Oδ1(Asn106)], both hydrogen bonds contributing to maintaining the structure of the tail in this position.

Structure of the [2Fe-2S] Cluster and Its Environment. The two Fe atoms are coordinated tetrahedrally by the two inorganic S atoms and four cysteinyl S atoms (Figure 4), as in the other 2Fe−Fds. The Sγ atoms of Cys42 and Cys48 are bonded to the iron atom that is close to the molecular surface, and those of Cys51 and Cys87 are bonded to the iron atom buried in the molecule. The orientation of the cluster in the molecule is conserved in the Fdx/Pdx subfamily and is similar to that in the plant-type Fd subfamily. The peptide segments in the vicinity of the [2Fe-2S] cluster are folded in such a way that the majority of the NH groups are directed to the cluster and the C═O groups to the surface of the molecule. Most side chains of the cluster-wrapping segment (Cys42−Cys51) are accessible to solvent. Of these, Cys46 in Fdx must be noted because its side chain has a reactive sulfhydryl group. Cys46 in Fdx is not conserved in Adx or Pdx (Leu in Adx and Ala in Pdx); therefore, Fdx should have biochemical behavior different from that of Adx or Pdx (discussed below). The hydrogen bond between the remote segments in Fdx [Nζ(Lys44)···Oδ(Asp29)] is reminiscent of that between Arg42 and Asp31 in the plant-type Fds [residue numbers are in *Spirulina platensis* Fd (*30*)]. This hydrogen bond is conserved in most plant-type Fds and may contribute to stabilizing the peptide conformation around the cluster.

NH···S hydrogen bonds are present in the vicinity of the [2Fe-2S] cluster of Fdx (Figure 4). In the current model, Nε2(Gln88) is close to Sγ(Cys87) (3.3 Å). But we are not certain that this contact is due to the NH···S hydrogen bond, because the present analysis could not rule out the possibility that the side chain of Gln88 has a different conformation in which the Cγ−Cδ bond is rotated by 180° so that the Oε atom is close to Sγ(Cys87). The hydrogen bond network scheme seen in Fdx is conserved in Adx and Pdx. In Fdx, however, it differs from that in the plant-type Fd subfamily, in which the deletion of one amino acid residue between the first and second cysteine residues (Cys42 and Cys48 in Fdx) relative to the Fdx/Adx subfamily has produced a different conformation for this peptide segment.

Electrostatic Potential. Figure 5 shows the electrostatic potentials on the surface of Fdx viewed in two directions. One side (Figure 5a) has two acidic areas and is in marked contrast to the other side (Figure 5b). One of these areas (A, upper right in Figure 5a) is composed of a segment that includes αF (Glu64, Glu67, Glu69, Asp71, and Asp74), and the other (B, lower left in Figure 5a) has segments that include αE, βG, and the loop before βH (Glu57, Asp60, Glu80, Glu82, Asp93, Glu94, and Asp95). These two acidic areas are clearly separated by a hydrophobic lane composed of Pro63, Phe59, Pro81, and Leu79 (from lower right to upper left in Figure 5a). Although the corresponding surface shown in Figure 5a in Adx is negatively charged, it is less negative than that of Fdx, as anticipated from the sequence comparison (Figure 2). In particular, the negative feature of

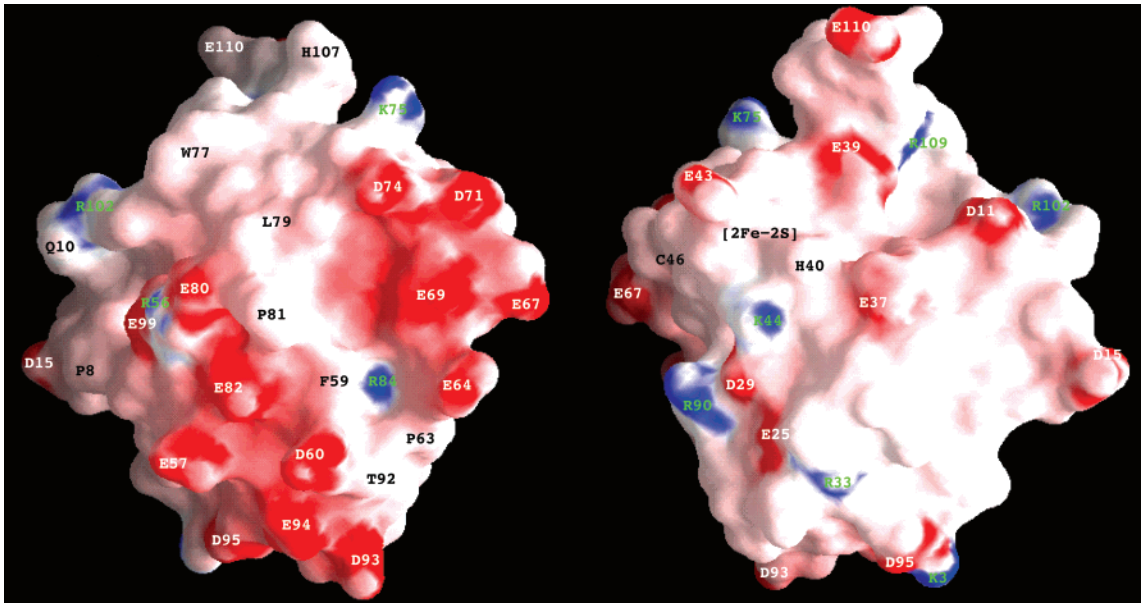

FIGURE 5: Distribution of electrostatic potentials on the surface of Fdx. Blue shows positive potentials and red negative ones. Panel b (right) is a view of Fdx rotated by 180° around the vertical axis relative to the view in panel a (left). The figures were drawn with GRASP (*50*).

area B in Adx (lower left in Figure 5a) is less prominent due to substitutions of the acidic residues in Fdx with neutral or basic residues in Adx.

Adx interacts with adrenodoxin reductase (AR) mainly by electrostatic interaction in which the negatively charged residues of Adx (Asp76 and Asp79) are involved (*43*). The crystal structure of the Adx−AR complex, prepared by cross-linkage of Adx Asp39 and AR Lys27, has shown that Asp72, Asp76, and Asp79 of Adx are indeed involved in the interaction with AR (*44*). Asp76 and Asp79 of Adx are conserved in Fdx, and Asp72 of Adx corresponds to Glu67 of Fdx (Figure 2). These are clustered in area A (upper right in Figure 5a). In contrast, area B is not involved in the interaction surface with AR in the cross-linked Adx−AR complex (*44*). Most acidic residues in area A in Fdx are also conserved in Pdx, in which chemical modification of these acidic residues has been shown to decrease its level of interaction with putidaredoxin reductase (PR) (*45*). The side chain of the conserved Glu69 in area A of Fdx extends along the surface molecule and forms a bridge to the side chain of the conserved Arg84 through two NH···O hydrogen bonds. Glu69 therefore may contribute to the stabilization of the tertiary structure. Indeed, in the cross-linked Adx−AR complex, the corresponding Glu74 of Adx faces away from the interface. The homologous protein (Yah1p) in *Saccharomyces cerevisiae* may also have a negatively charged surface that corresponds to area A (or αF) in Fdx on the basis of the sequence alignment (*15*). It appears, however, that the negative charge in area B in Fdx is not conserved in the Yah1p protein.

Putative Role of Fdx in the Assembly of Iron−Sulfur Clusters. Recent genetic studies have shown that disruption of the gene for *E. coli* Fdx or depletion of yeast Yah1p protein results in a marked decrease in the activities of various Fe−S proteins (*16*, *20*). In addition, overexpression of Fdx and other proteins encoded in the *isc* operon was demonstrated to enhance the cellular ability to assemble Fe−S clusters (*14*, *15*). So far, at least six proteins, including Fdx, have been identified as central components in the biogenesis of the Fe−S cluster (*16*−*18*), but little data are available for determining the molecular mechanism of the complex machinery and the functional role of Fdx in it. The analysis presented here has established that Fdx resembles Adx and Pdx in three-dimensional structure and the electrostatic potential of the putative interaction surface to the reductase. This suggests the possibility that Fdx interacts with reductase in a manner similar to those of the Adx−AR and Pdx−PR systems. Recent genetic studies on yeast Arh1p, the homologue of AR, consistently have shown its essential role in the assembly of Fe−S clusters (*46*). At present, the potential reductase partner of *E. coli* Fdx is not known.

The target of the electron transfer reaction mediated by Fdx/Yah1p has not been tested experimentally, but probable candidates include the reduction of S^0 to S^{2-} and Fe^{3+} to Fe^{2+}. Cysteine desulfurase IscS catalyzes the removal of sulfur from cysteine to form alanine and enzyme-bound S^0 (*47*), and the sulfane sulfur produced by IscS should be reduced to sulfide before combination with iron. The tertiary structure of Fdx shows that His40, Cys46, and His52 are located close to the [2Fe-2S] cluster (Figure 1). Of these, Cys46 in Fdx is noteworthy because it is conserved in the Yah1p protein, and the reactive sulfhydryl group of its side chain is on the molecular surface. In addition, the side chains of several hydrophilic residues (Ser66, Gln68, Glu69, and Gln88) are located near the sulfhydryl group of Cys46. We speculate that Cys46 is involved in the binding and reduction of S^0 and/or Fe^{3+}, but its precise role remains to be elucidated experimentally. Although His40 is located near the cluster, its involvement in binding Fe^{3+}/Fe^{2+} ions is less likely because Nδ(His40) is involved in hydrogen bonding to O(Ile38). There is no residue near the side chain of His40 that has the potential to stabilize the binding of His40 and these ions. His52 is buried inside the molecule. Takahashi and Nakamura discussed the possibility of conversion of the [2Fe-2S] cluster to the [3Fe-4S] or [4Fe-4S] cluster in the Fdx protein (*15*). The present conformation of its polypeptide,

however, is not suited to the accommodation of the [3Fe-4S] or [4Fe-4S] cluster with any combination of cysteine and histidine residues. Conversion of the cluster type, if at all, requires a large conformational change in the peptide wrapping the cluster.

Specific binding between Fdx and IscA has recently been reported (*48*). Although the exact role of IscA is unknown, it can bind the labile [2Fe-2S] cluster. IscA is an acidic protein (pI 4.6), but one-third of the N-terminal region is rich in basic residues (Arg12, Arg20, Lys22, Arg27, and Arg31). Acidic area A or B in Fdx therefore is assumed to bind to the N-terminal basic region of IscA. Because several basic residues are conserved in the corresponding regions in the IscA homologues of yeast (Isa1p and Isa2p), a candidate for the binding site with these proteins in Fdx/Yah1p is the conserved area A.

The crystal structure of Fdx presented here provides a sound base with which the function of Fdx is investigated by a method such as site-directed mutagenesis and finally a better understanding of the assembly mechanism of the iron−sulfur cluster in vivo.

ACKNOWLEDGMENT

We thank Drs. Masahide Kawamoto of JASRI, Nobuo Kamiya of RIKEN, and Noriyuki Igarashi and Mamoru Suzuki of the Photon Factory at Tsukuba for their valuable help with the data collection using synchrotron radiation. Part of this research was done with the approval of the SPring-8 Proposal Review Committee (Proposal 2000A0482-UL) and the Photon Factory Advisory Committee (Proposal 99G303).

REFERENCES

1. Beinert, H. (1990) *FASEB J. 4*, 2483−2491.
2. Matsubara, H., and Saeki, K. (1992) *Adv. Inorg. Chem. 38*, 223−280.
3. Holden, H. M., Jacobson, B. L., Hurley, J. K., Tollin, G., Oh, B. H., Skjeldal, L., Chae, J. K., Cheng, H., Xia, B., and Markley, J. L. (1994) *J. Bioenerg. Biomembr. 26*, 67−88.
4. Müller, J. J., Müller, A., Rottmann, M., Bernhardt, R., and Heinemann, U. (1999) *J. Mol. Biol. 294*, 501−513.
5. Usanov, S. A., Chashchin, V. L., and Akhrem, A. A. (1990) in *Frontiers in Biotransformation* (Ruckpaul, K., and Rein, H., Eds.) Vol. 3, pp 1−57, Akademie-Verlag, Berlin.
6. Peterson, J. A., and Graham-Lorence, S. E. (1995) in *Cytochrome P450: Structure, Mechanism and Biochemistry*, 2nd ed., pp 151−180, Plenum Press, New York.
7. Grinberg, A. V., Hannemann, F., Schiffler, B., Müller, J., Heinemann, U., and Bernhardt, R. (2000) *Proteins: Struct., Funct., Genet. 40*, 590−612.
8. Knaff, D. B., and Hirasawa, M. (1991) *Biochim. Biophys. Acta 1056*, 93−125.
9. Overington, J. P. (1992) *Curr. Opin. Struct. Biol. 2*, 394−401.
10. Orengo, C. (1994) *Curr. Opin. Struct. Biol. 4*, 429−440.
11. Pochapsky, T. C., Jain, N. U., Kuti, M., Lyons, T. A., and Heymont, J. (1999) *Biochemistry 38*, 4681−4690.
12. Müller, A., Müller, J. J., Muller, Y. A., Uhlmann, H., Bernhardt, R., and Heinemann, U. (1998) *Structure 6*, 269−280.
13. Zheng, L., Cash, V. L., Flint, D. H., and Dean, D. R. (1998) *J. Biol. Chem. 273*, 13264−13272.
14. Nakamura, M., Saeki, K., and Takahashi, Y. (1999) *J. Biochem. 126*, 10−18.
15. Takahashi, Y., and Nakamura, M. (1999) *J. Biochem. 126*, 917−926.
16. Tokumoto, U., and Takahashi, Y. (2001) *J. Biochem. 130*, 63−71.
17. Lill, R., and Kispal, G. (2000) *Trends Biochem. Sci. 25*, 352−356.
18. Mühlenhoff, U., and Lill, R. (2000) *Biochim. Biophys. Acta 1459*, 370−382.
19. Barros, M. H., and Nobrega, F. G. (1999) *Gene 233*, 197−203.
20. Lange, H., Kaut, A., Kispal, G., and Lill, R. (2000) *Proc. Natl. Acad. Sci. U.S.A. 97*, 1050−1055.
21. Knoell, H.-E., and Knappe, J. (1974) *Eur. J. Biochem. 50*, 245−252.
22. Jung, Y. S., Gao-Sheridan, H. S., Christiansen, J., Dean, D. R., and Burgess, B. K. (1999) *J. Biol. Chem. 274*, 32402−32410.
23. Ta, D. T., and Vickery, L. E. (1992) *J. Biol. Chem. 267*, 11120−11125.
24. Deleted in proof.
25. Leslie, A. G. W. (1992) *Joint CCP4 & ESF-EACBM Newsletter on Protein Crystallography*, No. 26, Daresbury Laboratory, Warrington, U.K.
26. CCP4 Collaborative Computational Project, No. 4 (1994) *Acta Crystallogr. D50*, 760−763.
27. Brünger, A. T., Adams, P. D., Clore, G. M., DeLano, W. L., Gros, P., Grosse-Kunstleve, R. W., Jiang, J. S., Kuszewski, J., Nilges, M., Pannu, N. S., Read, R. J., Rice, L. M., Simonson, T., and Warren, G. L. (1998) *Acta Crystallogr. D54*, 905−921.
28. Jones, T. A., Zou, J. Y., Cowan, S. W., and Kjeldgaard, M. (1991) *Acta Crystallogr. A47*, 110−119.
29. Laskowski, R. A., MacArthur, M. W., Moss, D. S., and Thornton, J. M. (1993) *J. Appl. Crystallogr. 26*, 283−291.
30. Fukuyama, K., Ueki, N., Nakamura, H., Tsukihara, T., and Matsubara, H. (1995) *J. Biochem. 117*, 1017−1023.
31. Tsukihara, T., Fukuyama, K., Mizushima, M., Harioka, T., Kusunoki, M., Katsube, Y., Hase, T., and Matsubara, H. (1990) *J. Mol. Biol. 216*, 399−410.
32. Ikemizu, S., Bando, M., Sato, T., Morimoto, Y., Tsukihara, T., and Fukuyama, K. (1994) *Acta Crystallogr. D50*, 167−174.
33. Rypniewski, W. R., Breiter, D. R., Benning, M. M., Wesenberg, G., Oh, B. H., Markley, J. L., Rayment, I., and Holden, H. M. (1991) *Biochemistry 30*, 4126−4131.
34. Jacobson, B. L., Chae, Y. K., Markley, J. L., Rayment, I., and Holden, H. M. (1993) *Biochemistry 32*, 6788−6793.
35. Bes, M. T., Parisini, E., Inda, L. A., Saraiva, L., Peleato, M. L., and Sheldrick, G. M. (1999) *Structure 7*, 1201−1211.
36. Frolow, F., Harel, M., Sussman, J. L., Mevarech, M., and Shoham, M. (1996) *Nat. Struct. Biol. 3*, 452−458.
37. Correl, C. C., Batie, C. J., Ballou, D. P., and Ludwig, M. L. (1992) *Science 258*, 1604−1610.
38. Vijay-Kumar, S., Bugg, C. E., and Cook, W. J. (1987) *J. Mol. Biol. 194*, 531−544.
39. Gronenborn, A. M., Filpula, D. R., Essig, N. Z., Achari, A., Whitlow, M., Wingfield, P. T., and Clore, G. M. (1991) *Science 253*, 657−661.
40. Nassar, N., Horn, G., Herrmann, C., Scherer, A., McCormick, F., and Wittinghofer, A. (1995) *Nature 375*, 554−560.
41. Pochapsky, T. C., Ye, X. M., Ratnaswamy, G., and Lyons, T. A. (1994) *Biochemistry 33*, 6424−6432.
42. Pikuleva, I. A., Tesh, K., Waterman, M. R., and Kim, Y. (2000) *Arch. Biochem. Biophys. 373*, 44−55.
43. Vickery, L. E. (1997) *Steroids 62*, 124−127.
44. Müller, J. J., Lapko, A., Bourenkov, G., Ruckpaul, K., and Heinemann, U. (2001) *J. Biol. Chem. 276*, 2786−2789.
45. Geren, L., Tuls, J., O'Brien, P., Millett, F., and Peterson, J. A. (1986) *J. Biol. Chem. 261*, 15491−15495.
46. Li, J., Saxena, S., Pain, D., and Dancis, A. (2001) *J. Biol. Chem. 276*, 1503−1509.
47. Flint, D. H. (1996) *J. Biol. Chem. 271*, 16068−16074.
48. Ollagnier-de-Choudens, S., Mattioli, T., Takahashi, Y., and Fontecave, M. (2001) *J. Biol. Chem. 276*, 22604−22607.
49. Evans, S. V. (1993) *J. Mol. Graphics 11*, 134−138.
50. Nicholls, A., Sharp, K. A., and Honig, B. (1991) *Proteins: Struct. Funct. Genet. 11*, 281−296.

BI010544T